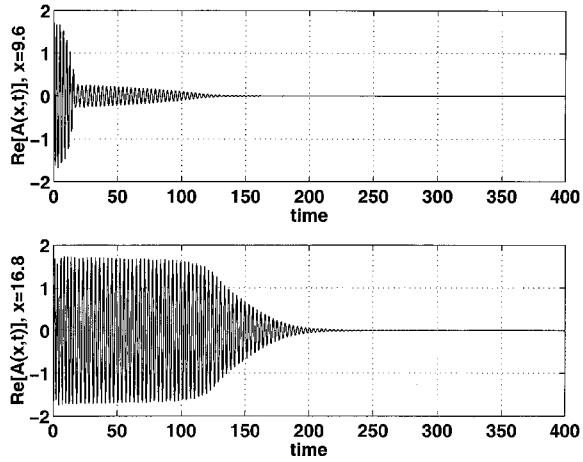

Fig. 2 Two-sensor feedback control at 12.5% above critical.

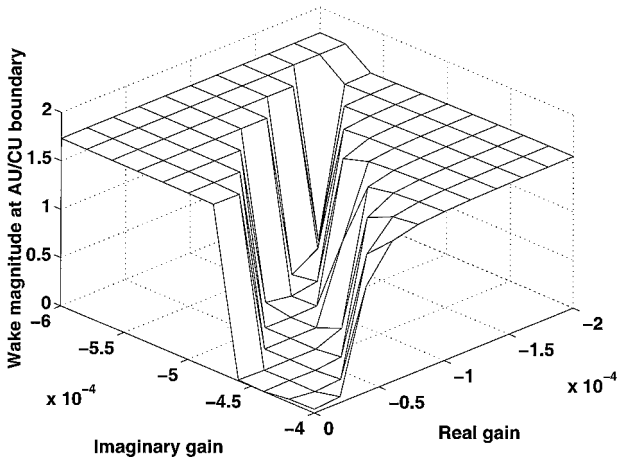

Fig. 3 Asymptotic wake magnitude for varying second sensor gain (12.5% above critical).

of 0.05, the figure shows which combinations of gain g_2 result in wake stabilization (corresponding to the zero asymptotic oscillation amplitude). This "window" of gains is quite small and shrinks with increasing μ_0. On either side of the gain window, there are plateaus: the left corresponding to oscillations in the original mode; the right to oscillations in another mode, destabilized by the control.

The dual-sensor control was found to be successful up to $\mu_2 = 3.876$ or 13% above criticality (compared to single sensor control, which fails at 5% above critical) even for a range of different sensor locations. It was conjectured that an increased number of distributed sensors might be able to extend this controllable range.

The feedback sensors employed in this study were at different streamwise locations, as this study is a preliminary investigation into stabilization of the two-dimensional cylinder wake. It is likely, however, that in a real wake, end effects will induce three-dimensional instabilities such that sensors placed at one spanwise location will fail to suppress vortex shedding at all spanwise locations.[3] For an actual wake sensors may need to be distributed in both spanwise and streamwise locations in the near wake.

Conclusions

Distributed sensing of the near wake of the globally unstable Ginzburg–Landau equation increases the controllable range of the wake. This was demonstrated by control of the wake further from criticality (13%) than possible before. This is a significant improvement in wake control, over single-sensor feedback schemes. It may be inferred that multiple, spatially distributed control schemes will increase the Reynolds number at which feedback control can stabilize the vortex shedding oscillations of the low-Reynolds-number cylinder wake.

There are large delays in the responses measured by the distributed sensors in the wake. Predictive controllers, rather than proportional feedback, may be a more appropriate strategy for future wake control strategies.

References

[1] Schumm, M., Berger, E., and Monkewitz, P. A., "Self-Excited Oscillations in the Wake of Two-Dimensional Bluff Bodies and Their Control," *Journal of Fluid Mechanics*, Vol. 271, 1994, pp. 17–53.

[2] Monkewitz, P. A., "Wake Control," *Bluff-Body Wakes, Dynamics and Instabilities*, edited by H. Eckelmann, Springer-Verlag, Berlin, 1992, pp. 227–240.

[3] Roussopoulos, K., and Monkewitz, P. A., "Nonlinear Modelling of Vortex Shedding Control in Cylinder Wakes," *Physica D*, Vol. 97, No. 1–3, 1996, pp. 264–273.

[4] Huerre, P., and Monkewitz, P. A., "Local and Global Instabilities in Spatially Developing Flows," *Annual Review of Fluid Mechanics*, Vol. 22, 1990, pp. 473–537.

[5] Roussopoulos, K., "Feedback Control of Vortex Shedding at Low Reynolds Numbers," *Journal of Fluid Mechanics*, 1993, pp 267–296.

[6] Park, D. S., Ladd, D. M., and Hendricks, E. W., "Feedback Control of von Karman Vortex Shedding Behind a Cylinder at Low Reynolds Numbers," *Physics of Fluids*, Vol. 6, No. 7, 1994, pp. 2390–2405.

[7] Park, D. S., Ladd, D. M., and Hendricks, E. W., "Feedback Control of a Global Mode in Spatially Developing Flows," *Physics Letters A*, Vol. 182, No. 2, 3, 1993, pp 244–248.

[8] Toro, E. F., "A Weighted Average Flux Method for Hyperbolic Conservation Laws," *Proceedings of the Royal Society of London A*, Vol. 423, No. 1865, 1989, pp. 401–418.

P. Givi
Associate Editor

Rapidly Growing Instability Mode in Trailing Multiple-Vortex Wakes

Jason M. Ortega* and Ömer Savaş†
University of California, Berkeley, Berkeley, California 94720-1740

I. Introduction

FOLLOWING Crow's[1] analytical study of the long-wave instability for a counter-rotating vortex pair, numerous wake-alleviation concepts have been tested in an effort to hasten this instability mechanism.[2–5] The hypothesis was that if this instability could be externally forced to grow, the linking of oppositely signed tip vortices would form Crow rings, hence, changing the two-dimensional nature of the wake into a three-dimensional one. The resulting incoherent wake would have an accelerated destruction, causing it to pose less of a threat to following aircraft. However, one drawback of the Crow instability is its slow growth rate. Typically, it requires a few hundred wingspans to develop, making it a less attractive candidate for rapid wake attenuation. The primary reason for this slow growth rate is that the equal-strength, oppositely signed vortices are too widely spaced for this cooperative instability to occur rapidly. To circumvent this impediment and increase the growth rate, it is necessary to redesign the trailing vortex wake.

One means of accomplishing this is to construct a vortex wake that contains multiple vortex pairs, each of which has vortices that are located close to one another. This allows the vortices to develop cooperative instabilities and interact strongly in a timescale much shorter than that for a single, widely spaced pair.[6] Recent towing tank experiments[7,8] have demonstrated this in the merger process of like-signed vortex pairs. By the mere reduction of the spacing between the flap and tip vortices from one-third of a span to one-sixth of a span, the vortices could interact more strongly

Received 15 January 2000; revision received 30 October 2000; accepted for publication 30 October 2000.

*Graduate Student, Department of Mechanical Engineering. Student Member AIAA.

†Professor, Department of Mechanical Engineering. Associate Fellow AIAA.

with each other and quickly develop instabilities, decreasing the downstream distance to merger from 70 to only 10 spans. Another means is to generate oppositely signed vortices that have unequal strengths, resulting in a vortex wake that can decay by means other than the Crow instability.[1] Corsiglia and Dunham[9] present numerical results from a vortex filament code[10] in which unequal-strength, oppositely signed flap vortices develop a sinusoidal instability that quickly grows to a finite size. Recently, Quackenbush et al.[11–13] have numerically explored a concept called vortex leveraging for alleviating the sailplane wake of a submarine. By periodically introducing control vortices by means of shape memory alloys, the flap vortices from the sailplane are spatially perturbed, causing them to interact with the oppositely signed tip vortices at downstream distances of 20–30 spans. Experimental verification, however, does not seem to be available at the present time.

To test these two concepts, a series of flow visualization experiments were conducted. This Note presents the results of these tests and describes a class of instabilities that is seen both within an unequal strength, counter-rotating vortex pair and between the vortex pairs on either side of a wing. We observe that a trailing vortex wake that has undergone this instability exhibits the formation of three-dimensional structures much sooner than the wake following the growth of the classical Crow instability.[1]

II. Experimental Setup

Two wings (Fig. 1) are employed for these experiments: a rectangular wing (Fig. 1a) that serves as the control wing, which provides a reference against which the other wing is compared, and a wing that has triangular tip flaps (Fig. 1b). The wings are made of curved sheet metal of thickness 3.2 mm and both have a span $b = 40$ cm, chord $c = 6.7$ cm, and camber radius $R = 17$ cm. The triangular flap extensions have widths of $d = 0.25b$. The leading and trailing edges are tapered and rounded to minimize flow separation. The experiments are performed at the University of California at Berkeley Richmond Field Station towing tank facility. The tank measures 2.4 m wide by 70 m long and has a nominal water depth of 1.5 m. For this particular series of tests, an aluminum carriage is towed behind a motorized one, allowing a better top-view of the vortices from the instant they formed. The wings are attached to the aluminum carriage by a streamlined, stainless steel strut, which places them approximately 0.5 m beneath the water surface. Recent particle image velocimetry (PIV) measurements[7] demonstrated that strut had minimal influence on the formation and ensuing dynamics of the wake vortices.

Flow visualization is performed by applying a mixture of fluorescent sodium salt (Sigma Chemical Company, Number F-6377) and corn syrup to the upper surface of the wings at the flaps and wing tips in 2.5-cm-wide strips (Fig. 1). To increase the amount of time that this dye mixture lasts in the water, it is simmered over a heat source so that the majority of the water content is removed, giving it the consistency of hardened caramel. The dye is washed into the boundary layer on the top surface of the wing. The dyed fluid meets the fluid from the lower surface boundary layer to form the three-dimensional vortex sheet in the wake of the wing. Because the molecular diffusivity of water is much smaller than its momentum diffusivity, the dye remains as a partial marker of the vortex sheet, which rapidly rolls up into vortices. The dye is not a complete marker of the sheet because the wing is partially painted with it. Hence, we argue that in the rolled up wake, all of the dye marks vorticity, but not all vorticity is marked by the dye. At larger downstream distances, only coherent structures that correlate well with themselves both spatially and temporally are discussed. Therefore, if a large dispersal of dye is observed in the wake, no attempt is made to relate this to a large dispersal of vorticity.

The test section, located about halfway down the length of the tank, is illuminated by passing a 10-W continuous wave laser beam through a spherical lens. The light cone thus generated allows for volumetric visualization of the flowfield. A video camera is positioned about a meter upstream of the test section and views the wings and trailing vortices through the water surface. The surface waves generated by the strut cause some image distortion, but this does not have any significant effects on the flow observations. Additional flow visualization images are obtained by viewing the trailing vortices through the side windows of the test section.

For each run, the wing is towed at a velocity $U = 1.6$ m/s ($Re_c = Uc/\nu = 1.07 \times 10^5$, where ν is the kinematic viscosity of water) and at an angle of attack $\alpha = 2.0$ deg. Because of the different planform areas of the wings, the circulation strengths of the resulting wakes vary somewhat between the wings, though their values are of the same order of magnitude. Because the purpose of this study is to investigate the qualitative features of the wakes, these slight differences should not present a problem. The carriage begins its motion 20 m upstream of the test section and continues until it reaches the end of the tank. Typically, 20 min are allowed to pass between runs, allowing the water in the tank to become quiescent. A total of seven flow visualization tests are performed: two with the rectangular wing having no flaps and five with the wing having triangular flaps.

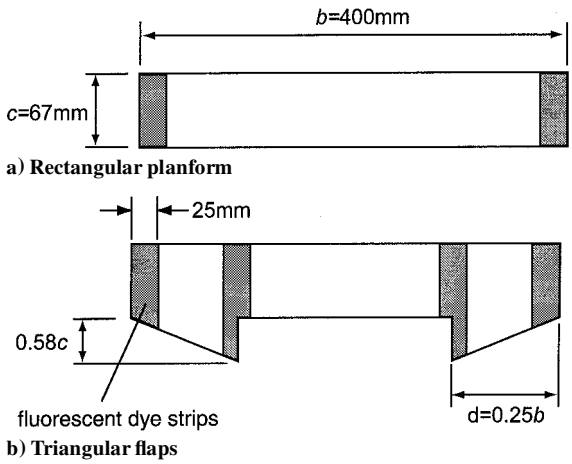

Fig. 1 Wing planforms.

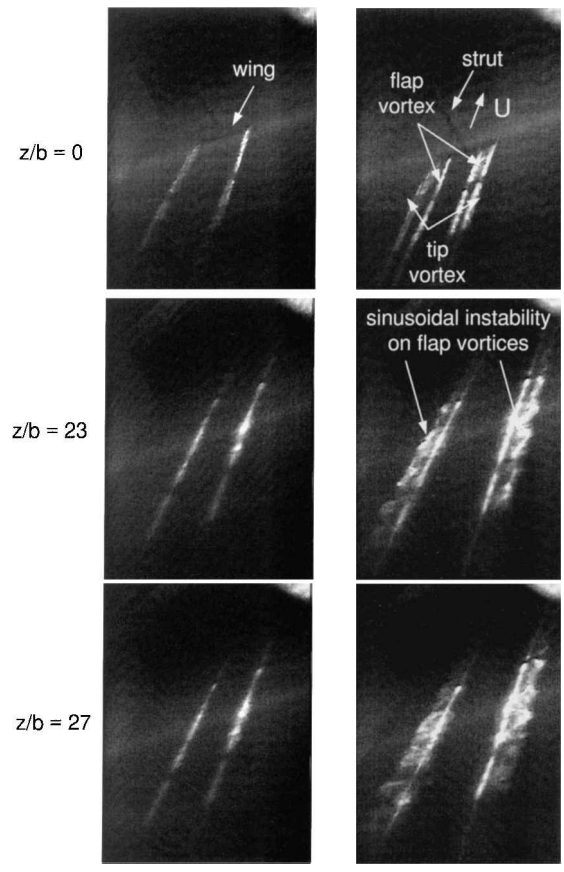

Fig. 2 Video sequences with wing in view in the first frame ($z/b = 0$) of each column.

III. Observations

Sequences of flow visualization images from video tape recordings are shown in Fig. 2 for both wings. The columns correspond to images from the rectangular wing and the triangular-flapped wing. The rows correspond to the different downstream distances z/b from the wings. The $z/b = 0$ frames show the wings just as they pass through the center of the test section. The streamwise ripples visible at $z/b = 0$ are the optical distortions due to the surface waves generated by the strut.

The first column in Fig. 2 shows the counter-rotating vortex pair in the wake of the rectangular wing. This sequence of images is taken as the basis for comparison with the outboard-flapped wing experiments discussed later. Consistent with earlier studies in this facility[7,8] using the rectangular wing, the vortices shed from it indicate no signs of a long-wave instability during the observations. The vortices simply descend quietly until they proceed below the illuminated portion of the test section ($z/b = 150$, not shown). Observations of the rectangular wing's wake at much later times do show initial signs of the long-wave Crow instability.[1] However, by this time, the wing has stopped and the vortex pair is nearing the tank floor. The behavior of the pair, therefore, is not investigated further.

The vortex wake of the wing with triangular flaps is shown in the second column of Fig. 2. The tip vortices have the same senses of rotation as those for the rectangular wing, whereas each of the flap vortices have a sense of rotation that is opposite to that of the nearby tip vortices. Thus, two counter-rotating vortex pairs are generated.

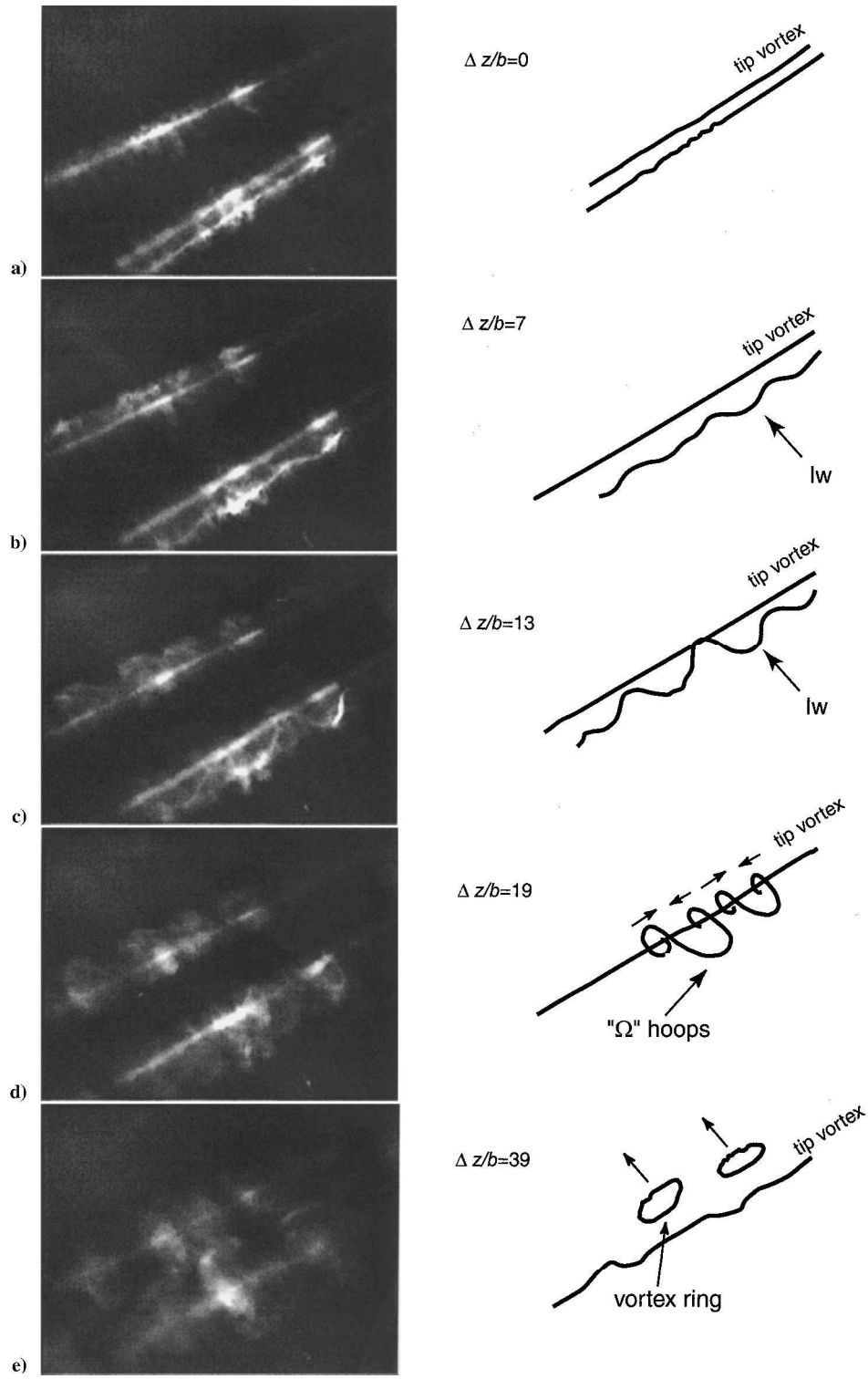

Fig. 3 Instability mode-detail: photographs and outlines of dye concentrations; $\Delta z/b$ indicates the relative separation in each frame.

An estimate of the vortex strength ratios can be made by observing the paths of the vortices in a pair. The vortex pair rotates around its vorticity centroid in the reference frame of the descending wake. The initial separation of the pair and the location of their common centroid uniquely determine the ratio of their strengths. Because the midportion of the wing produces lift, the flap and tip vortices are of unequal strength, resulting in a circulation ratio $|\Gamma_{\text{flap}}/\Gamma_{\text{tip}}| < 1$, where $\Gamma_{\text{flap, tip}}$ are the vortex circulations.

The flowfield from the triangular-flapped wing is markedly different than that of the rectangular wing. After forming, the oppositely signed flap and tip vortices begin their interaction by orbiting around their common vorticity centroid, which lies outboard of the wing tips. The pair essentially clears the geometric wake, the downstream region through which the wing has previously traveled. At approximately 20 spans, the weaker flap vortices, which have now moved outboard, develop a sinusoidal instability in the wake of the triangular-flapped wing. The wavelength of this stationary instability is about one span or four times the initial separation distance of the flap and tip vortices. As the amplitude of the instability grows, the flow becomes nonlinear, and the periodic portions of the flap vortices closest to the tip vortices are advected inboard and rapidly wind around the tip vortices ($z/b = 27$).

IV. Details of the Instability Mode

To better illustrate the instability development and the subsequent nonlinear vortex interactions, Fig. 3 shows closeup images in the wake of the triangular-flapped wing. The images in the left column are taken from a video sequence that is recorded at a slightly different angle than those in Fig. 2. Note that the downstream locations of the frames are labeled as $\Delta z/b$ and not z/b. The right column was drawn following the observations of the dye streaks of the starboard pair in those sequences. In a manner similar to the preceding discussion, the flap and tip vortices orbit outwardly about their vorticity centroid. By the time the pair has rotated about π rad, a long-wavelength, sinusoidal instability develops on the weaker flap vortices. The long-wave instability, which is a cooperative mode, alters the nature of the vortices and quickly becomes the central event in the wake (Figs. 3b–3e). As the instability progresses, the peaks on the flap vortices become tightly wrapped around the tip vortices, forming Ω-shaped hoops (Fig. 3d). The shape of the vortex pair just before the formation of these hoops is similar to that in Fig. 13 of Klein et al.[14] The spiral feet of these hoops advect themselves toward one other, causing the hoops to form closed vortex rings (Fig. 3e). These rings are then hurled toward the opposite side of the wake. It is clear that this long-wave instability (lw) is a member of a more general class of modes for arbitrary strength vortices. When the vortices are of the same sign, the vortex pair is linearly stable.[15] However, when the vortices are of opposite sign, the instability grows rapidly, as is evident in these flow visualization images.

V. Growth Rate of the Instability Mode

We estimate the growth rate of the instability shown in Fig. 2 to compare it with the growth rates of other instabilities that exist between a single pair and multiple pairs of trailing vortices. When the image of the wing at $z/b = 0$ is used as a reference length, the amplitude of the instability at $z/b = 23$, at which time the flap vortex has orbited about π rad about the tip, is found to be approximately 6 cm. The amplitudes of the initial disturbances on the trailing vortices are taken to be on the order of the boundary-layer thickness at the trailing edge of the flap. As conservative estimate, if we approximate the flow over the wing by that of a turbulent boundary layer over a flat plate, the boundary-layer thickness is $0.37 \cdot x \cdot (Ux/\nu)^{-1/5} = 0.35$ cm, where $x = 1.58c = 10.6$ cm (Schlichting).[16] With this information, the growth rate α of the instability can be found from the expression $y = y_0 e^{\alpha t}$, where $y = 6$ cm is the perturbation amplitude at 23 spans, y_0 is the initial amplitude, and $t = (23 \text{ spans}) \times (40 \text{ cm/span})/(160 \text{ cm/s})$. Solving this expression for α yields a growth rate of $0.5\ \text{s}^{-1}$.

To compare the growth rate of this instability with that of the Crow[1] instability, it is necessary to calculate the characteristic timescale $\tau_d = 2\pi d^2/\Gamma_{\text{tip}}$ of a single vortex pair. By performing this exercise, as done by Bristol,[17] it is possible to compare the instability growth rate with the rate of strain, $\Gamma_{\text{tip}}/2\pi d^2$, from the neighboring tip vortex. To estimate Γ_{tip}, the root circulation about the wing is first estimated as $\Gamma_0 = 250\ \text{cm}^2/\text{s}$ from preliminary PIV measurements in the wake of the wing with triangular flaps. Next, we utilize the equation for the distance $\underline{x}$ between the flap vortex and the vorticity centroid of the vortex pair. This can be found from the expression $x_c = \frac{1}{2}(\beta - b) + d = d\Gamma_{\text{tip}}/\Gamma_0$, where β is the distance between the vorticity centroids on either half of the wing. Computing the average distance between the tip vortices from $z/b = 0$ to 23 demonstrates that β is about equal to 45 cm. Substituting the values of β, Γ_0, and d into the expression for $\underline{x}$ shows that $\Gamma_{\text{tip}} = 313\ \text{cm}^2/\text{s}$, giving a characteristic timescale of 2.0 s and a dimensionless growth rate of $\gamma_d = 2.0\ \text{s} \cdot 0.5\ \text{s}^{-1} = 1.0$. When scaled in this manner, the estimated growth rate of this instability is on the order of that predicted by Crow[1] for two equal-strength, oppositely signed vortices.

From an aircraft design point of view, the dimensionless growth rate can also be compared to that of a wing with multiple vortices. For this purpose, we define another characteristic timescale as that by Crouch,[6] which is $\tau_\beta = 2\pi\beta^2/\Gamma_0 = 51$ s. With this scaling, the dimensionless growth rate of the counter-rotating pair is $\gamma_\beta = 51\ \text{s} \cdot 0.5\ \text{s}^{-1} = 25$. The instability growth rate of a wake with multiple corotating pairs is taken to be 1.5 (Ref. 6), the value for the A_2 mode (see Fig. 3a of Ref. 6 with $\delta = 0.3$ and $\Gamma_{\text{flap}}/\Gamma_{\text{tip}} = 0.5$). These values of δ and $\Gamma_{\text{flap}}/\Gamma_{\text{tip}}$ give a ratio of $d/b = 0.25$, allowing a rough comparison to be made with the triangular-flapped wing used in this study. Note that the growth rate of the instability in Fig. 2 is about 17 times greater than that of the A_2 mode given by Crouch.[6] The growth rate data are summarized in Table 1. PIV measurements are being conducted to provide a more quantitative assessment of the wakes of these wings.[18]

Table 1 Instability growth rates

Γ_f/Γ_t	γ_d	γ_β	Source
0	0.8	——	Crow[1]
+0.5	——	1.5	Crouch[6]
−0.2	1	25	Present experiments

VI. Summary

A rapidly growing instability mode is observed between unequal, oppositely signed vortices in the wakes of wings. Having a wavelength of about one wingspan, this instability develops on the weaker flap vortices at approximately 20 spans downstream of the wing. All that is necessary to excite this instability is to place two unequal, oppositely signed vortices close to one another, where they can interact strongly. The rapid growth of the instability and the exchange of vorticity across the wing centerline suggest that this instability might be utilized as a means of controlling the vortex wake and, perhaps, reducing the wake hazard.

Acknowledgments

We thank R. Bristol and L. Tsuei for their helpful discussions in this work.

References

[1] Crow, S. C., "Stability Theory for a Pair of Trailing Vortices," *AIAA Journal*, Vol. 8, No. 12, 1970, pp. 2172–2179.

[2] Chevalier, H., "Flight Test Studies of the Formation and Dissipation of Trailing Vortices," *Journal of Aircraft*, Vol. 10, No. 1, 1973, pp. 14–18.

[3] Dunham, R. E., Jr., "Unsuccessful Concepts for Aircraft Wake Vortex Minimization," *NASA Symposium on Wake Vortex Minimization*, edited by A. Gessow, NASA SP-409, 1976, pp. 221–250.

[4] Barber, M. R., and Tymczyszyn, J. J., "Wake Vortex Attenuation Tests: A Status Report," *1980 Aircraft Safety and Operating Problems*, NASA CP-2170, 1981, pp. 387–408.

[5] Rossow, V. J., "Lift-Generated Vortex Wakes of Subsonic Transport Aircraft," *Progress in Aerospace Sciences*, Vol. 35, No. 6, 1999, pp. 507–660.

[6] Crouch, J. D., "Instability and Transient Growth for Two Trailing-Vortex Pairs," *Journal of Fluid Mechanics*, Vol. 350, 1997, pp. 311–330.

[7] Bristol, R., Ortega, J., and Savas, Ö., "Towing Tank Study of Airfoil Wake Vortices at Re_Γ of Order 10^5," AIAA Paper 99-3419, June 1999.

[8] Chen, A., Jacob, J., and Savas, O, " Dynamics of Corotating Vortex Pairs in the Wakes of Flapped Airfoils," *Journal of Fluid Mechanics*, Vol. 383, 1999, pp. 155–193.

[9]Corsiglia, V. R., and Dunham, R. E., "Aircraft Wake Vortex Minimization by Use of Flaps," *NASA Symposium on Wake Vortex Minimization*, edited by A. Gessow, NASA SP-409, 1976, pp. 305–338.

[10]Leonard, A., "Numerical Simulation of Interacting, Three-Dimensional Vortex Filaments," *Proceeding of the 4th International Conference on Numerical Methods in Fluid Dynamics*, Boulder, CO, 1974, pp. 245–250; *Lecture Notes in Physics*, Vol. 35, Springer-Verlag, Berlin, 1975, pp. 245–250.

[11]Quackenbush, T. R., Bilanin, A. J., and McKillip, R. M., Jr., "Vortex Wake Control Via Smart Structures Technology," *Proceedings of the SPIE—The International Society for Optical Engineering*, Vol. 2721, SPIE, Bellingham, WA, 1996, pp. 78–92.

[12]Quackenbush, T. R., Bilanin, A. J., Batcho, P. F., McKillip, R. M., Jr., and Carpenter, B. F., "Implementation of Vortex Wake Control Using SMA-Actuated Devices," *Proceedings of the SPIE—The International Society for Optical Engineering*, Vol. 3044, SPIE, Bellingham, WA, 1997, pp. 134–146.

[13]Quackenbush, T. R., Batcho, P. F., Bilanin, A. J., and Carpenter, B. F., "Design, Fabrication, and Test Planning for an SMA-Actuated Vortex Wake Control System," *Proceedings of the SPIE—The International Society for Optical Engineering*, Vol. 3326, SPIE, Bellingham, WA, 1998, pp. 259–271.

[14]Klein, R., Majda, A. J., and Damodaran, K., "Simplified Equations for the Interaction of Nearly Parallel Vortex Filaments," *Journal of Fluid Mechanics*, Vol. 288, 1995, pp. 201–248.

[15]Jimenez, J., "Stability of a Pair of Co-Rotating Vortices," *Physics of Fluids*, Vol. 18, No. 11, 1975, pp. 1580, 1581.

[16]Schlichting, H., *Boundary-Layer Theory*, 7th ed., McGraw–Hill, New York, 1979, p. 638.

[17]Bristol, R. L., "Co-Operative Wake Vortex Instabilities," Ph.D. Dissertation, Univ. of California, Berkeley, CA, Dec. 2000.

[18]Ortega, J. M., "Stability Characteristics of Counter-Rotating Vortex Pairs in the Wakes of Triangular-Flapped Airfoils," Ph.D. Dissertation, Univ. of California, Berkeley, CA, May 2001.

A. Plotkin
Associate Editor

Influence of Boundary-Layer Thickness on Base Pressure and Vortex Shedding Frequency

A. Rowe,* A. L. A. Fry,* and F. Motallebi†
University of London,
London, England E1 4NS, United Kingdom

Nomenclature

C_{pb}	=	base pressure coefficient, $(p_b - p_s)/0.5\rho u^2$
f	=	vortex shedding frequency
H	=	boundary-layer shape factor, δ^*/θ
h	=	trailing-edge thickness
p_b	=	base pressure
p_s	=	static pressure at traverse position
Sr_h	=	Strouhal number, fh/u
u	=	freestream velocity
δ	=	boundary-layer thickness based on 99.5% of freestream velocity
δ^*	=	boundary-layer displacement thickness
θ	=	boundary-layer momentum thickness
ρ	=	density

Introduction

VORTEX shedding in the wake of bluff bodies is an important flow phenomenon. At subsonic and transonic speeds, it has long been recognized that the wake behind an isolated two-dimensional section with a blunt trailing edge may break into a vortex street. The direct result of this is an increase in drag, mainly as a result of reduced base pressure.[1–3] Several investigators have reported on the factors affecting the base drag and vortex shedding,[4–7] that is, base geometry, base bleed, state of the boundary layer at the trailing edge, etc. The objective of present study was to experimentally investigate the influence of the thickness of turbulent boundary layers upstream of trailing edge on the base pressure and vortex shedding frequency and for a given boundary-layer state (turbulent in this case) to determine the predominant parameters that affect the base drag and vortex shedding frequency. Further, unlike previous investigations,[1–7] where the change in the boundary-layer characteristics (thickness and/or state) has been brought about mainly as a result of change in Reynolds number and/or Mach number, in the present work the Reynolds number and Mach number were kept constant and the change in the boundary-layer thickness has been brought about by introducing roughness elements.

Experimental Setup and Procedures

The experiments were conducted at zero pressure gradient and at two speeds. The low-speed experiments (nominal freestream velocity of 23 m/s) were performed in a closed-circuit wind tunnel with a 1.0×0.77 m rectangular section of length 2.30 m. The model (Fig. 1) consisted of a flat plate, 0.05 m thick, 0.77 m wide, and 1.0 m long with an elliptical leading edge and a square cut trailing edge. The nominal freestream Reynolds number based on the model's chord length was 1.7×10^6. To change the thickness of the boundary layer before the separation point, wires with different diameters were placed symmetrically at the end of the leading-edge curvature on both sides of the model. In total three wires with diameters of 1.62, 2.4, and 3.4 mm were used. The high-speed tests were conducted in a transonic wind tunnel with slotted walls. The tunnel has a working section of 8.9×16.5 cm. The tests were carried out at a freestream Mach number of 0.68. The freestream Reynolds number based on the chord of the model was about 2.15×10^6. The model used in high-speed tests was essentially similar in design with that of the low-speed test and had an elliptic leading edge followed by a straight rectangular section, as shown in Fig. 1. The high-speed experiments were carried out for only two boundary-layer thicknesses (with and without roughness element).

Measurement of the boundary-layer profiles was made at a point upstream of the trailing edge (see Tables 1 and 2), where the surface static pressure on the model begins to decrease as the blunt trailing edge is approached. The total pressure across the boundary layer was measured using flat-ended pitot probes. The static pressure across the boundary layer was assumed to be constant and equal to the pressure recorded by the surface pressure tap. The physical boundary-layer thickness was defined as the distance perpendicular to the model surface where the velocity was approximately 0.995 of the local freestream velocity. Tables 1 and 2 give the details of the boundary-layer parameters determined from the experimental surveys of the boundary layer. No corrections were made to account for the displacement effects of the pitot tube. Temperature compensated piezoresistive pressure sensors (Scanivalve digital sensor arrays, Model DSA 3017) were used for pressure measurements. The low-pressure model (pressure range ±2.5 kPa) had an accuracy of ±0.3% and the high-pressure model (pressure range −100–690 kPa) had an accuracy of ±0.08%. The measurement of the vortex shedding frequency was carried out by placing a hot-wire probe behind the trailing edge of the model. The location of the probe tip was slightly above the model surface (this position was slightly different for each test case to get the best periodic signals, but was within the 10% of the base height) at a distance of approximately half of the base height behind the trailing and in the center-span plane of the models. The

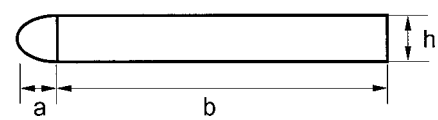

Fig. 1 Schematic profile of experimental model; low-speed model: $a = 10$, $b = 90$, and $h = 5$; high-speed model: $a = 2.5$, $b = 10$, and $h = 1$ (dimensions are in centimeters).

Received 2 February 2000; revision received 27 November 2000; accepted for publication 28 November 2000.

*Student, Department of Engineering, Queen Mary.
†Lecturer, Department of Engineering, Queen Mary.